



Cross-ripple patterns and wave directional spectra

Richard A. Cheel¹ and Alex E. Hay¹

Received 11 January 2008; revised 26 May 2008; accepted 27 June 2008; published 11 October 2008.

[1] Rotary sonar images of the seafloor during SandyDuck97 are used to investigate the geometry of the cross-rippled bed state relative to the directional properties of the incident waves. The sonar imagery indicates that the cross-ripple pattern is a quasi-regular diamond-shaped lattice constructed of variable length ladder-like tiles, each with shorter-wavelength ripples residing within the troughs of the longer-wavelength component. The longer-wavelength crests were oriented at approximately $\pm 30^\circ$ with respect to the incident wave direction. Most wave directional spectra were not bimodal in direction and, for the small number (17%) which were, the distribution of the angular separations of the two peaks was very broad and indicated no preferred value. Thus, contrary to some previous suggestions in the literature, these results indicate not only that cross ripples do not require waves propagating from two different directions for their formation but also that for most of the occurrences during this experiment, cross ripples formed when the incident wave field was unimodal in direction. Finally, the orientation angles of the long-crested ripple components exhibit no dependence on mean current velocity.

Citation: Cheel, R. A., and A. E. Hay (2008), Cross-ripple patterns and wave directional spectra, *J. Geophys. Res.*, *113*, C10009, doi:10.1029/2008JC004734.

1. Introduction

[2] The first definitive observations of cross ripples in wave-dominated, sandy, nearshore environments appear to have been made by Clifton *et al.* [1971]. These bed forms are composed of two sets of ripples, each set having a different characteristic wavelength and orientation, and are thus intrinsically three-dimensional (3-D). As described by Clifton *et al.* [1971], the long-wavelength ripple set has “long, straight, uninterrupted crests,” with short-wavelength, short-crested ripples sitting in the troughs of the longer set, and with the crests of the two sets approximately orthogonal so that the two sets together form a “ladder-like” pattern (Figure 1). The angle between the two sets of ripple crests was reported to be approximately bisected by the incident wave direction. Machida *et al.* [1974] described a similar “ladder-like” bed form which also consisted of long, straight, parallel crests with shorter-crested, shorter-wavelength ripples between the longer crests. The presence of two primary spatial scales, and the 3-D character of the ripple pattern, complicate the conceptual picture of sand ripple formation under the action of surface gravity waves. For example, if cross ripples are generated under essentially unidirectional waves as has been suggested [Clifton *et al.*, 1971; Machida *et al.*, 1974], they would not readily conform to the orbital-suborbital-anorbital classification scheme proposed by Clifton and Dingler [1984] for 2-D wave-formed ripples.

[3] Cross ripples have been observed in the nearshore zone visually using SCUBA [Clifton *et al.*, 1971; Machida *et al.*, 1974; Doucette, 2000], a compound comb device [Machida *et al.*, 1974], and in sonar images during single storm events [Hay and Wilson, 1994; Smyth *et al.*, 2002]. More recently, Hay and Mudge [2005] summarized bed state occurrences during the SandyDuck97 experiment, also observed using rotary sonars. Cross ripples were one of 5 principal bed states, occurring in 10% of the sonar images over a ~ 75 day period. Cross ripples were identified as a principal bed state not only because of their relatively high frequency of occurrence but also because they occurred repeatably during both the growth and decay phases of individual storm events, at wave energies intermediate between irregular and linear transition ripples. They were not relic features, occurring instead during active transport conditions. Thus, the SandyDuck97 observations indicate that cross ripples represent an integral part of the bed state storm cycle, and the implications are that cross-ripple occurrence is (1) independent of prior bed state and, (2) consequently, to first order, a function solely of the hydrodynamic forcing conditions.

[4] In the cross-shore bed state progression proposed by Clifton [1976], cross ripples occur at intermediate wave energies. Similarly, cross ripples occur at intermediate wave energies in the bed state storm cycle [Hay and Wilson, 1994; Smyth *et al.*, 2002; Hay and Mudge, 2005]. Thus, there is a substantial and growing body of evidence for the wave energy conditions under which cross ripples occur. The same is not the case for wave direction, however. Clifton *et al.* [1971] and Clifton [1976] noted that although cross ripples resemble interference ripples, waves were not incident from two directions when cross ripples were observed.

¹Department of Oceanography, Dalhousie University, Halifax, Nova Scotia, Canada.

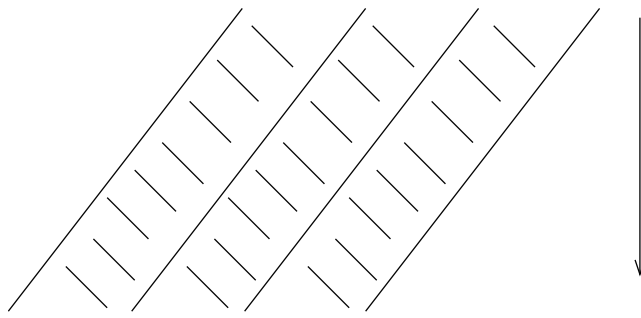


Figure 1. Schematic indicating the ladder-like appearance of cross-ripples described by *Clifton et al.* [1971], *Machida et al.* [1974], and *Clifton* [1976]. Arrow indicates the reported wave direction, i.e., bisecting the $\sim 90^\circ$ intersection angle between long and short crests.

(Interference ripples form through “the action of two coexisting but differently oriented trains of waves” *Allen* [1984]). In fact, *Clifton et al.* [1971] definitively state that the cross-ripple pattern they observed “is not produced by waves approaching from two different directions.” *Machida et al.* [1974] similarly remarked that the waves were not obviously bidirectional during their cross-ripple occurrences. Nevertheless, citing the *Clifton et al.* [1971] and *Machida et al.* [1974] observations, *Allen* [1984, p. 452] states that the “strengthening of short-crestedness as waves shoal provides a satisfactory explanation” for their “interference-like” ripples. Short-crestedness arises from the directional distribution of wave energy. Outside the surf zone (where cross ripples occur), field observations indicate that the directional distribution of shoaling random waves tends to become narrower toward shore due to refraction [*Herbers et al.*, 1999], implying that wave short-crestedness would be expected to decrease shoreward. Thus, it is unclear how the explanation given by *Allen* would normally apply. Nonetheless, the wave directions reported by *Clifton et al.* [1971] and *Machida et al.* [1974] were based on visual observations. Thus, a quantitative basis for examining possible relationships between cross-ripple occurrence and wave directional distributions is lacking.

[5] This paper sets out to investigate the geometric properties of cross-ripple patterns relative to the directional properties of the incident wave field. A primary focus is the orientation of cross-ripple crests relative to peaks in the wave directional spectrum. Using the extensive data set compiled by *Hay and Mudge* [2005], the expectation is that with cross-ripple occurrences from $O(10)$ separate storm events, it should be possible to determine whether intersecting wave trains are required for cross-ripple formation.

[6] The methods used to analyze the data are outlined in section 2. The results, in section 3, begin with the signature pattern of cross ripples as revealed in the sonar imagery. Estimates of the wavelength of the long- and short-ripple components computed via spectra of the sonar images are presented. The orientation angle of the long-crested component is compared with the dominant wave direction and with the mean longshore and cross-shore currents. Wave directional spectra during cross-ripple occurrences are pre-

sented. The implications of the results are discussed in section 4 and concluding remarks are made in section 5.

2. Field Site and Data

[7] *SandyDuck97* took place from August to November 1997 at the U. S. Army Corps of Engineers Field Research Facility (FRF) in Duck, North Carolina (see *Birkemeier et al.* [1985] for a detailed description of the FRF site). The results presented here are from instrument frames C and D located 270 and 310 m offshore (Figure 2). The water depths at these two locations remained approximately constant: 3.36 ± 0.05 m and 3.29 ± 0.05 m at C and D, respectively. Images of the seabed were acquired with 2.25 MHz rotary fan beam sonars (transducers approximately 0.73 m above the bed) at 30 min intervals between storm events and 10 min intervals during storms. Water velocities were measured using Marsh-McBirney EM flowmeters approximately 0.35 m above the bed. The flowmeters were sampled at a rate of 2 Hz in half hour intervals continuously. Further details on the instrumentation are given by *Henderson and Bowen* [2002] and *Hay and Mudge* [2005].

[8] Figure 3 presents rms horizontal velocities in the sea-and-swell band (that is frequencies between 0.05 and 0.3 Hz) at both locations, with cross-ripple occurrences superimposed. Cross ripples occurred for rms wave orbital velocities between 10 and 40 cm/s (with a mean and standard deviation of 18 ± 3 cm/s [*Hay and Mudge*, 2005]).

[9] Figure 4 is a sonar image showing a cross-rippled bed typical of the *SandyDuck97* data. Ripple properties were obtained from the sonar images using two methods. The first method is based on 2-D power spectra, determined as follows. The left region of the sonar image was divided into eight boxes (each 3.4 m \times 3.4 m) with 68% nominal overlap (Figure 5). The subimage in each box was high-pass filtered (fifth-order Butterworth filter, 0.67 cpm cutoff frequency), and Hanning windowed in both x and y direc-

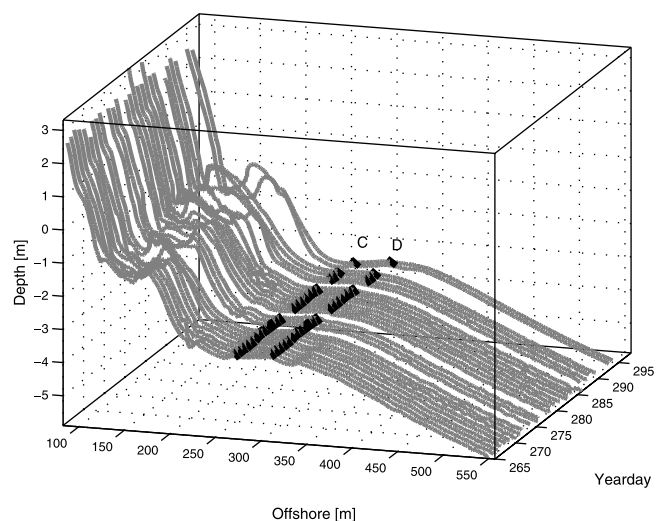


Figure 2. Time series of bed elevation profiles past the locations of instrument frames C and D during *SandyDuck97*. Note that the depth and bed profile at the frame locations remained roughly constant through time.

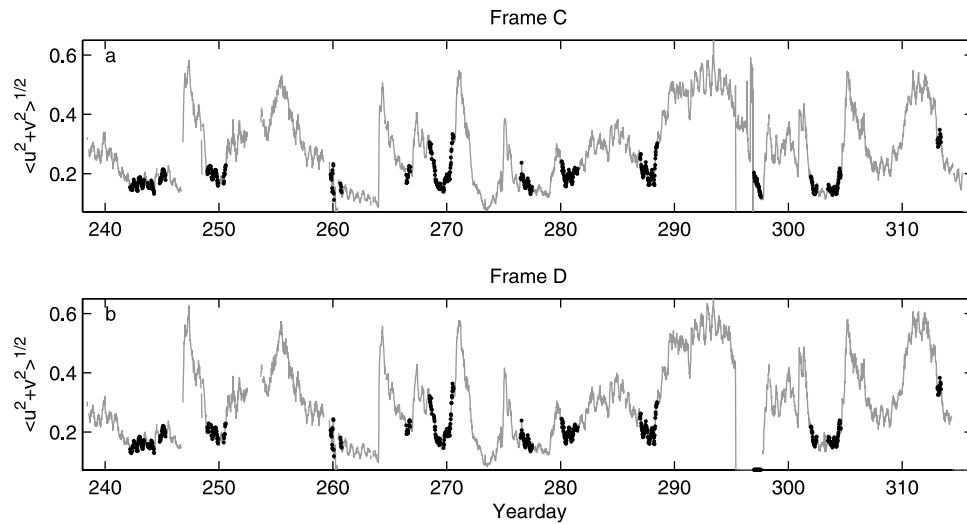


Figure 3. Time series of rms horizontal wave orbital velocities at frames (a) C and (b) D. Black dots correspond to times when cross ripples are observed in the sonar record. Adapted from *Hay and Mudge* [2005].

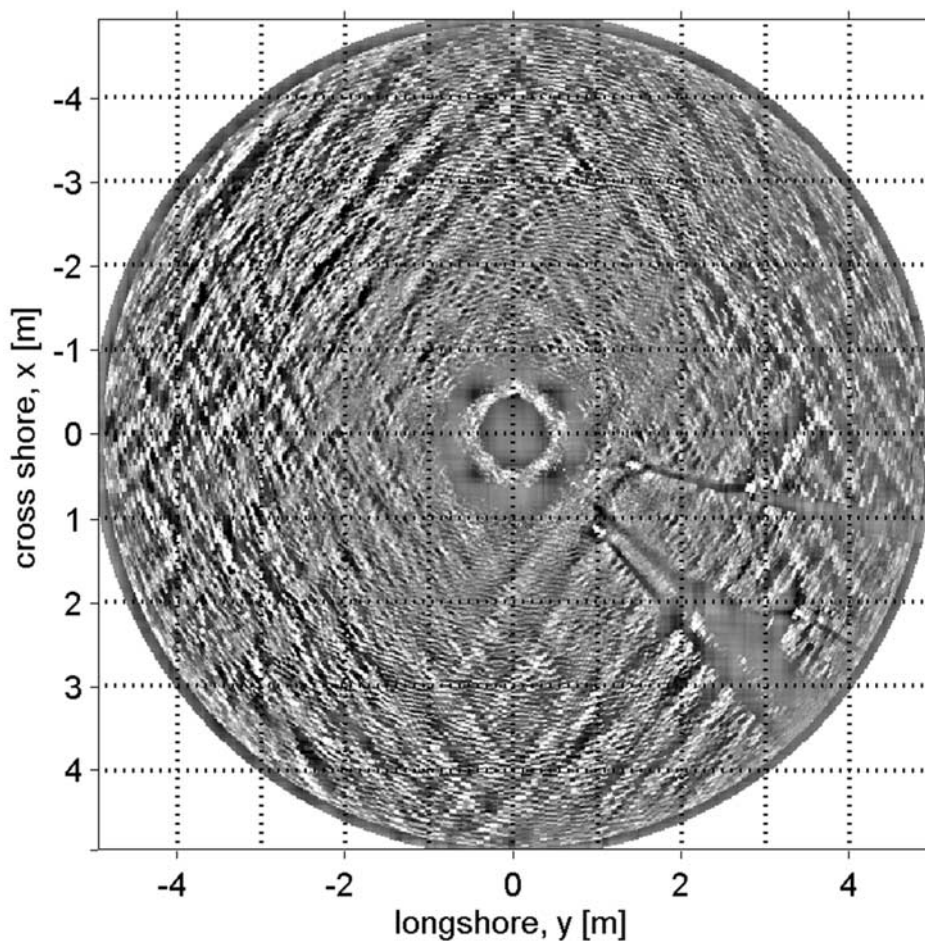


Figure 4. Rotary fan beam sonar image illustrating the characteristic cross-ripple pattern. Note that the orientation of the long-crested component of cross ripples varies from quadrant to quadrant. Acoustic shadows cast by the instrument frame legs can be seen in the lower right quadrant. Top is offshore. Image resolution is 1.8 cm. The image has been high-pass filtered (0.67 cpm cutoff) to remove the low-frequency variations due to the transducer beam pattern.

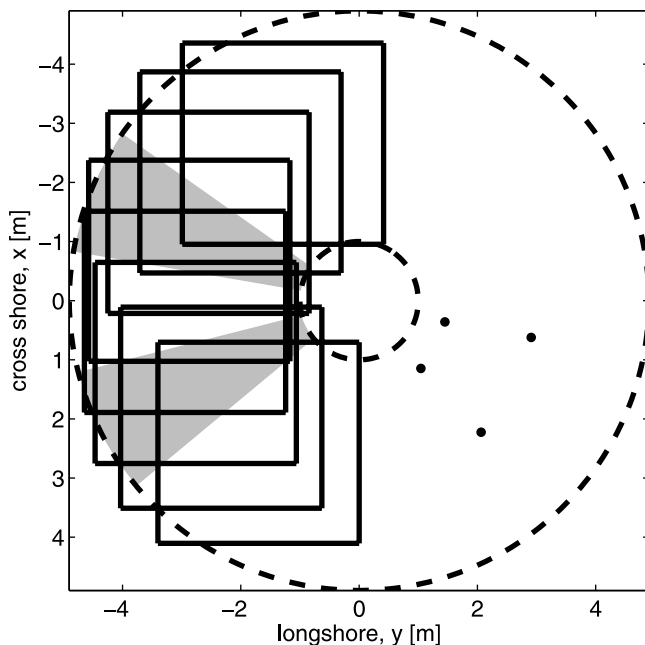


Figure 5. Cartoon depicting the areas of the sonar images used in the spectral analyses. The sea bed is imaged in the area between the dashed circles. The solid black circles denote the instrument frame legs. The eight boxes, each $3.4 \text{ m} \times 3.4 \text{ m}$, indicate the areas of the image used to compute the 2-D power spectrum. The grey shaded areas correspond to the sectors over which the average radial spectra were determined.

tions. Note that though the corners of some of the boxes extend beyond the sonar image, the Hanning window forces the values at the edges of the boxes to be essentially zero. The 2-D power spectra within each box were ensemble averaged. An example ensemble-average spectrum is presented in Figure 6a (k and l denote onshore and longshore wave numbers, respectively) and shows four main lobes in the directional distribution of backscatter variance. These four lobes correspond to directions normal to ripple crests: that is, the variance of the seafloor backscatter is largest in these directions. The negative onshore wave number region containing all of the independent information in the power spectrum is shown in Figure 6b, as are the computed orientation angles, ψ_{L1} and ψ_{L2} .

[10] The orientation angles are computed from the locations in wave number space of the two maxima in the spectrum:

$$\psi = \arctan(|k|/l). \quad (1)$$

ψ_{L1} corresponds to the orientation angle of the long-crested ripples with positive longshore wave numbers; ψ_{L2} to the angles of long-crested ripples with negative longshore wave numbers. The red and black solid lines in Figure 6b pass through the energy maxima from which the orientation angles were computed. (Note that the 2-D spectrum is dominated by the low wave number signal corresponding to the long-crested component, so the wavelengths and orientation angles of the short-crested component could not be unambiguously distinguished from noise.)

[11] The second method involves sector-averaged radial spectra and was used for estimating ripple wavelengths. The radial spectra were averaged over sectors 24.5° wide centered on azimuthal angles of -67° and -117° relative to 0° onshore (the two shaded regions in Figure 5). These sectors were chosen to be centered upon the area where the cross ripples were typically the best resolved and where the signal from 2-D ripple types (e.g., linear transition ripples) did not mask the signal from the short-crested component. An example sector-averaged radial spectrum is shown in Figure 7 along with the corresponding ripple wavelengths. The short-crested ripple wavelengths were identified with the maximum spectral density in the wave number range of $7.5 < K \leq 25$ cpm, long-crested wavelengths with the peak spectral density in the range $1 \leq K < 7.5$ cpm.

[12] Dominant wave direction was computed from the sea-and-swell band of the cross-shore, u , and alongshore, v , velocities following *Fofonoff* [1969]:

$$\tan 2\theta_o = \frac{2\langle uv \rangle}{\sigma_u^2 - \sigma_v^2}, \quad (2)$$

where the angle brackets denote the time average, and (σ_u^2, σ_v^2) are the (u, v) variances. Wave directional spectra, $\mathbb{S}(f, \theta)$, were also computed from the flowmeter measurements of u, v and pressure, p , using the Iterative Maximum Likelihood Method (IMLM) [*Oltman-Shay and Guza, 1984*].

[13] Wave directional spectra from the 8-m array are also used here. These directional spectra are similarly based on an IMLM estimator [*Long, 1991*] and were shoaled to the locations of the instrument frames assuming constant cross-shore energy flux [*Bowen, 1969*]. The spectra were then transformed from the surface to the measurement depth according to linear wave theory.

[14] Both estimates of the wave directional spectra were classified into those that were bimodal and those that were not. A directional spectrum was determined to be bimodal in direction if the 1-D integral,

$$D_\theta = \int \mathbb{S}(f, \theta) d\theta, \quad (3)$$

was found to have two peaks and the ratio of the central minimum to the smaller peak was less than $8/\pi^2$ (the Rayleigh criterion [*Jenkins and White, 1957*]). Similarly, the integral of the directional spectrum over wave direction,

$$D_f = \int \mathbb{S}(f, \theta) d\theta, \quad (4)$$

was used to determine if the spectrum was bimodal in frequency.

3. Results

3.1. Cross-Ripple Pattern

[15] Owing to the nature of the rotary fan beam sonar, ripple features are best resolved when the crests are orthogonal to the acoustic beam. Thus, in certain regions of the sonar image in Figure 4, the long-crested components are more easily seen than the short-crested components,

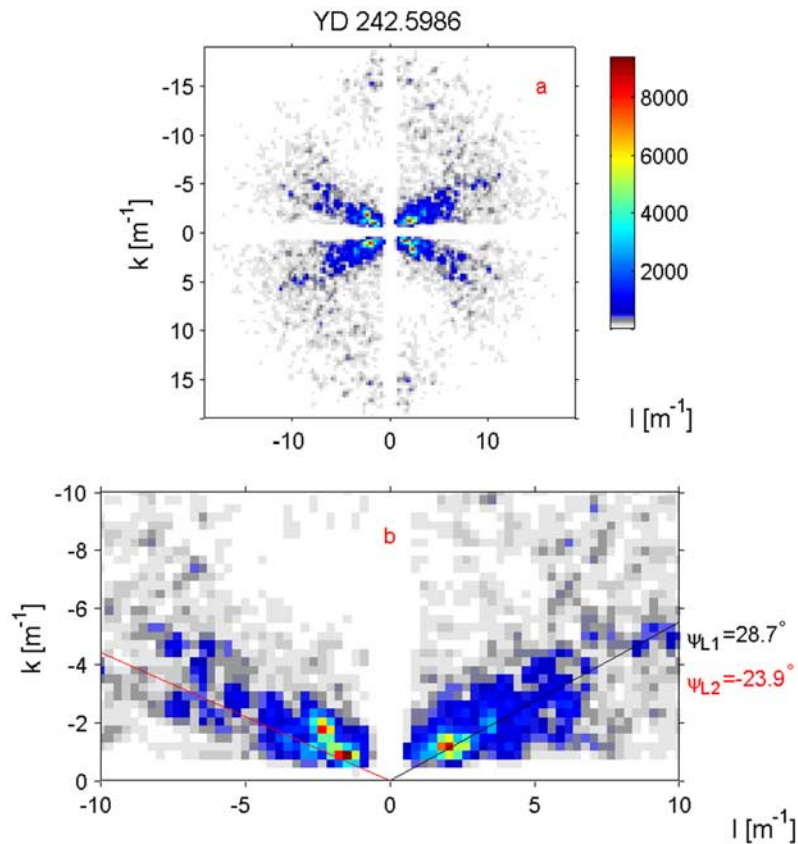


Figure 6. (a) Example ensemble-averaged 2-D power spectrum of a typical cross-ripple image. The four lobes, only two of which are independent, correspond to high backscatter from ripple crests. (b) Closeup of the negative (onshore) wave number region which contains all of the independent information. Here ψ_{L1} and ψ_{L2} denote the orientation angles of long-wavelength, long-crested ripples with positive and negative longshore wave numbers.

likewise the opposite is true in other regions. Figure 8 shows examples of images in which cross ripples were the dominant bed form. In each case, the region shown is from the left side of the full image, well away from the instrument frame. The ladder-like features characteristic of cross ripples are most easily seen in Figure 8a in the region around $(x, y) = (-3.5, -1)$ m. In the observations reported by Clifton *et al.* [1971] the crests of the short- and long-crested ripple sets were reported to be approximately perpendicular, with the dominant set having “long, straight, uninterrupted crests.” In the cross-ripple occurrences during SandyDuck97, the long-crested components were usually present in two orientations and typically crossed or intersected each other, leading to a diamond-like pattern (e.g., Figure 8b) at larger (≥ 0.5 m) scales. The angle between the short- and long-crested ripples during SandyDuck97 was estimated to be approximately 60° (see Figure 8a near $(x, y) = (-3, -1)$ m), rather than the $\sim 90^\circ$ angles reported in other studies [e.g., Clifton *et al.*, 1971; Doucette, 2000].

3.2. Ripple Wavelengths and Orientations

[16] A definition sketch of the ladder-like substructure of the cross-ripple pattern observed in the sonar imagery is presented in Figure 9. The variables λ_L and λ_S denote the wavelengths of the long-crested “rails” and the short-crested “rungs.” Here ψ_L is the angle between the shore

normal and the rails and is positive counterclockwise from the shore normal (x) axis.

[17] Wavelengths and orientations for the long-crested ripple components obtained from the 2-D power spectra

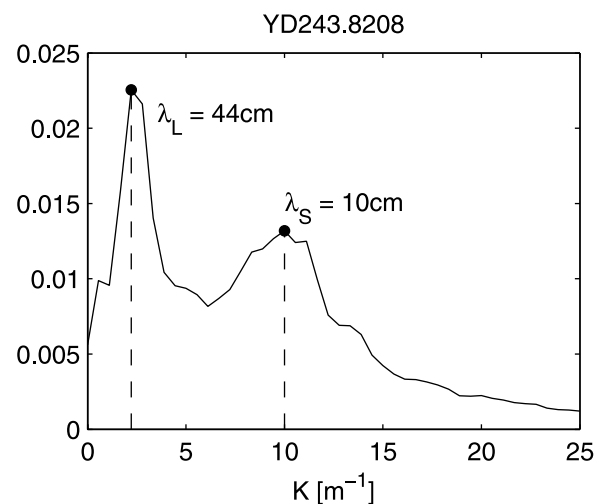


Figure 7. Example of a sector-averaged radial spectrum used to compute λ_L and λ_S , the wavelengths of the long- and short-crested components of cross ripples, respectively.

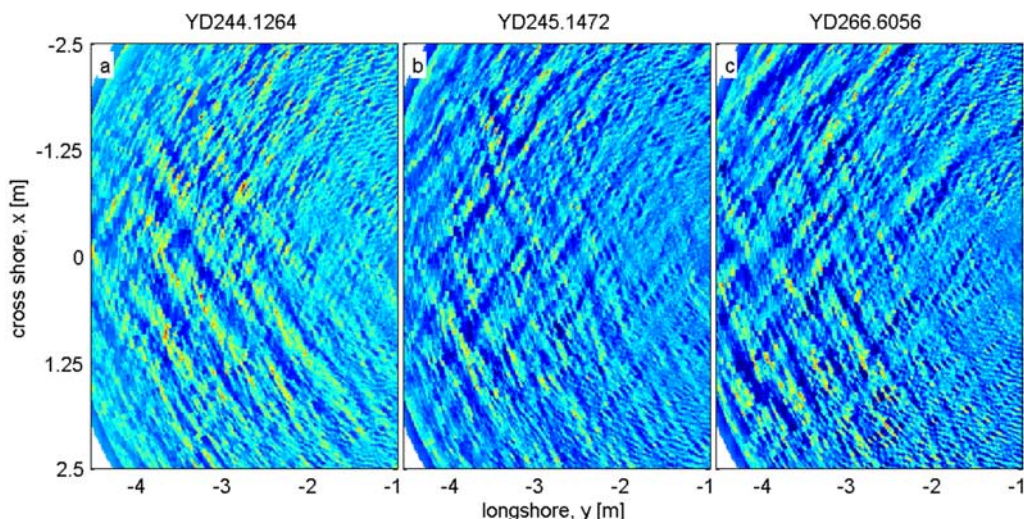


Figure 8. Selected sonar images showing typical instances of the cross-ripple pattern. Region of image shown corresponds to the northern side of the instrument frame (see Figure 4). The images were high-pass filtered, with a 0.67 cpm cutoff.

are listed in Table 1. The wavelengths for the long-crested component in either orientation are much the same, as are the magnitudes of the orientation angles. The results at the two frame locations are also comparable. The radial spectra provide wavelength estimates for both the long- and short-crested components and are also listed in Table 1. The estimates of the long-crested ripple wavelength from both

methods are consistent, indicating a typical wavelength of 30 to 50 cm. The short-crested ripple wavelengths were about 10 cm. These wavelength estimates are consistent with those found in the literature: *Hay and Wilson [1994]* reported long-crested ripple wavelengths of 30 to 40 cm, and *Doucette [2000]* reported wavelengths of 10 to 70 cm, and 7 to 15 cm, for the long- and short-crested components, respectively.

[18] The distributions of ψ_{L1} and ψ_{L2} are presented in Figure 10, with maximum values of 30° and -23° . Thus, the angle between the long-crested components with positive and negative longshore wave numbers was typically 50° to 60° . The ripple crest bisector, defined as $(\psi_{L1} + \psi_{L2})/2$, was typically around 5° from shore normal. Given the 5° to 10° probable error in sensor alignment relative to the shoreline, this number is not significantly different from zero.

[19] The dominant wave direction, θ_o , and peak directions from the *puv* and the shoaled 8-m array directional spectra are also included in Figure 10. The offset between the *puv* and 8-m array wave directions is probably due to misalignment of the EM flowmeters relative to the frame. The wave directions bisected the long-crested ripples to within the $\pm 5^\circ$ uncertainty in the data.

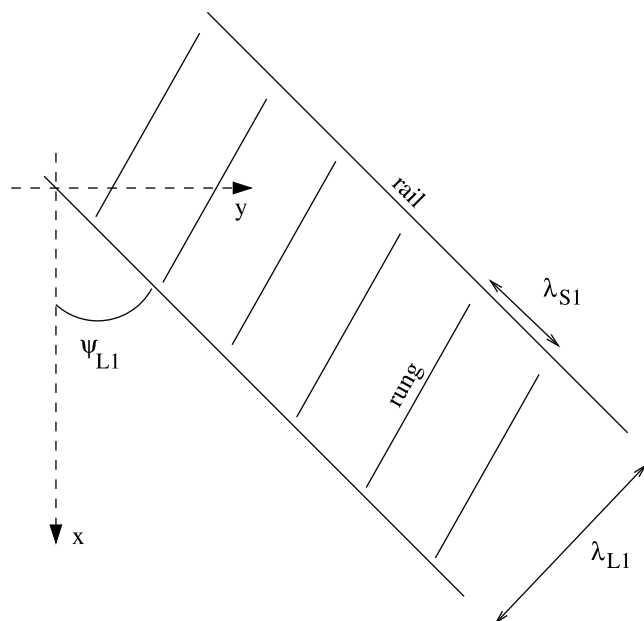


Figure 9. Sketch of the ladder-like pattern characteristic of cross ripples, with definitions of wavelengths of the long- and short-crested components, λ_L and λ_S and long crest angle, ψ_L . The subscript 1 denotes crests with a positive crest angle (and positive longshore wave number). Cross ripples with negative crest angle, ψ_{L2} , would be represented by the mirror image of the above cartoon in the x axis. Positive x is shoreward.

Table 1. Cross-Ripple Wavelengths and Orientations^a

	Frame C	Frame D
<i>Two-Dimensional Spectra</i>		
N	714	769
λ_{L1}	39 ± 17 cm	36 ± 19 cm
λ_{L2}	41 ± 15 cm	30 ± 15 cm
ψ_{L1}	$36.6 \pm 15.4^\circ$	$39.8 \pm 16.7^\circ$
ψ_{L2}	$-27.8 \pm 10.2^\circ$	$-38.7 \pm 18.5^\circ$
<i>Radial Spectra</i>		
N	757	807
λ_L	44 ± 21 cm	55 ± 38 cm
λ_S	9.6 ± 0.2 cm	9.8 ± 0.2 cm

^aErrors represent standard deviation from the mean. N refers to the number of sonar images upon which the statistics are based.

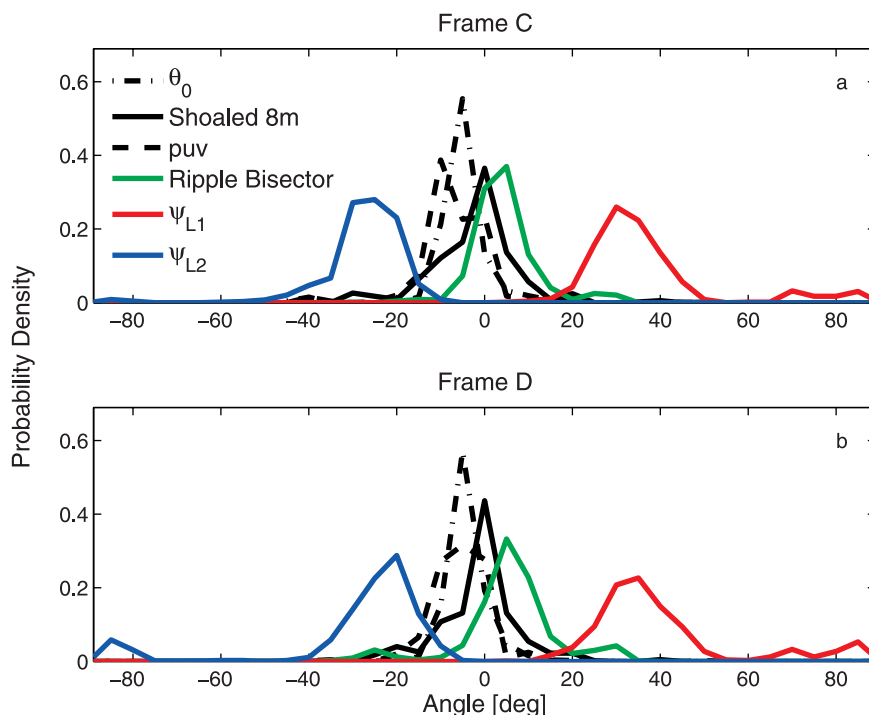


Figure 10. Distributions of ψ_{L1} and ψ_{L2} , the orientation angles for the long-crested ripples; the dominant wave direction, θ_o (equation (2)); the peak wave direction from the shoaled 8-m array directional spectra; the peak wave direction from the p_{uv} wave directional spectra; and the ripple bisector. from frames (a) C and (b) D.

[20] Time series of cross-ripple crest orientation, computed from the 2-D power spectra, for two cross-ripple occurrences are presented in Figure 11. The first time interval is between Yeardays 242.3 and 243.5 (Figure 11a). During this period, orientation angles exhibit $\pm 10^\circ$ variations about their mean values but no tendency for these means to evolve with time. The wave energy during this period also remained approximately constant (Figure 3). During the second time interval, Yeardays 249.1 to 249.4 (Figure 11b), the ripples with negative crest orientation angles also did not vary significantly in orientation. The crests with positive crest angles, however, did evolve with time, decreasing through-

out the time interval. During this interval the wave energy gradually diminished (Figure 3). Thus, the crest orientations of these bed forms were quasi-stationary, but they did evolve through time.

3.3. Ripple Crest Orientation Versus Mean Current Speed

[21] The variation of ψ_L with mean onshore current, U , and mean longshore current, V , is presented in Figures 12a and 12b, respectively. For the majority of the cross-ripple occurrences, $|U|$ and $|V|$ were less than or equal to 0.05 m/s and 0.1 m/s, respectively. These mean current speeds are

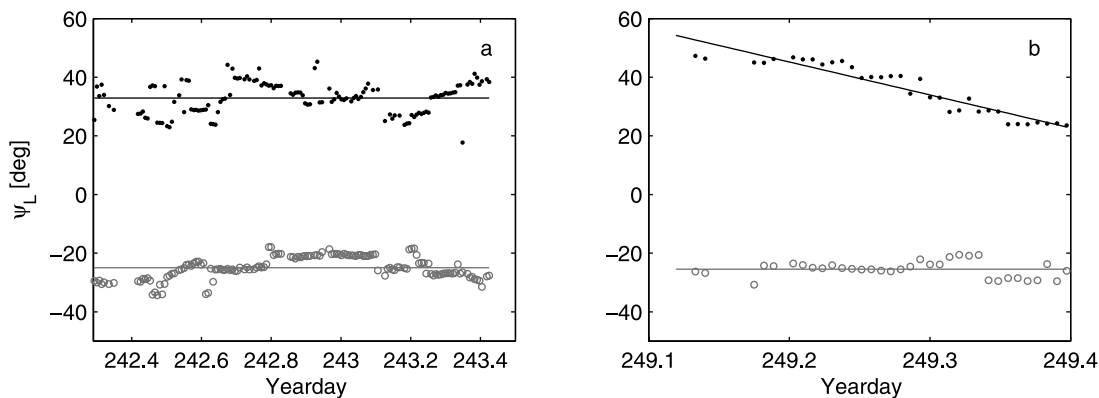


Figure 11. (a and b) Time series of cross-ripple crest orientation angle for two time intervals. Black points and gray circles denote ripple crests with positive and negative crest angles, respectively. Horizontal lines correspond to mean values, the sloped line in Figure 11b shows linear fit to crest orientation angle. Data are from frame C.

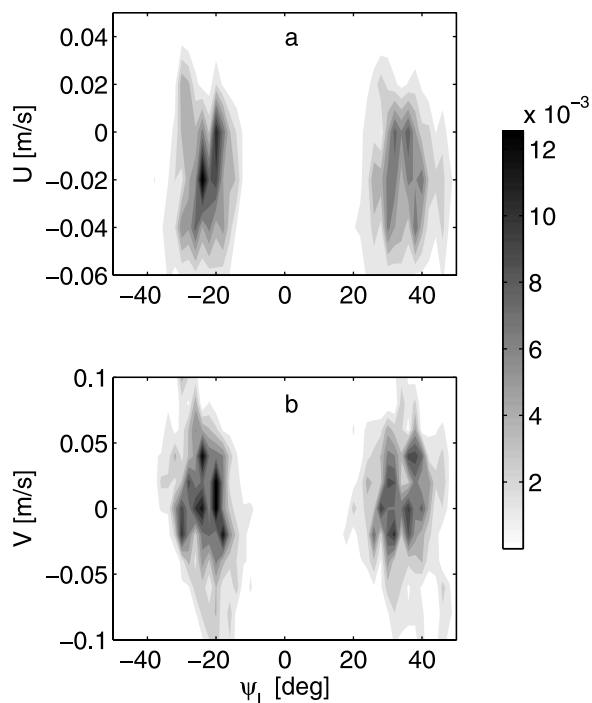


Figure 12. Two-dimensional histograms of mean (a) cross-shore and (b) longshore currents versus ψ_L from frames C and D. Color bar denotes fractional occurrence of cross ripples at a specific mean current and crest angle.

low compared to the approximately 40 cm/s average significant wave orbital velocity. Thus, one would expect the cross-rippled bed state in these data to be wave-dominated. Consistent with this expectation, Figure 12 indicates no dependence of crest angle on mean currents.

3.4. Wave Directional Spectra

[22] Figure 13 presents the wave directional spectra averaged over all cross-ripple occurrences for both frames. Data from the 8-m array and the p_{uv} directional spectra are presented. As stated previously, the 8-m array spectra have been shoaled to the frame locations assuming constant shore normal energy flux, and transformed to the bottom using linear wave theory. The p_{uv} spectra were estimated from the EM flowmeter data at each frame. Prior to averaging over the cross-ripple occurrences, each spectrum was normalized by its pressure variance (σ_p^2) in the sea-and-swell band. At both locations as well as for both the shoaled 8-m array and p_{uv} data, the directional spectra were unimodal, on average. The mean frequency and directional spread were similar at both locations and for both methods. That is, at frame C, the half widths at half maximum mean spectral density were $\pm 15^\circ$ and $\pm 13^\circ$ in direction, and ± 0.025 Hz and ± 0.028 Hz in frequency for the shoaled 8-m array and the p_{uv} data, respectively. The corresponding values at frame D were $\pm 14^\circ$ and $\pm 12^\circ$, and ± 0.025 and ± 0.022 Hz. However, cross ripples did sometimes occur when the directional spectrum was bimodal: Figure 14 shows one such instance, in this

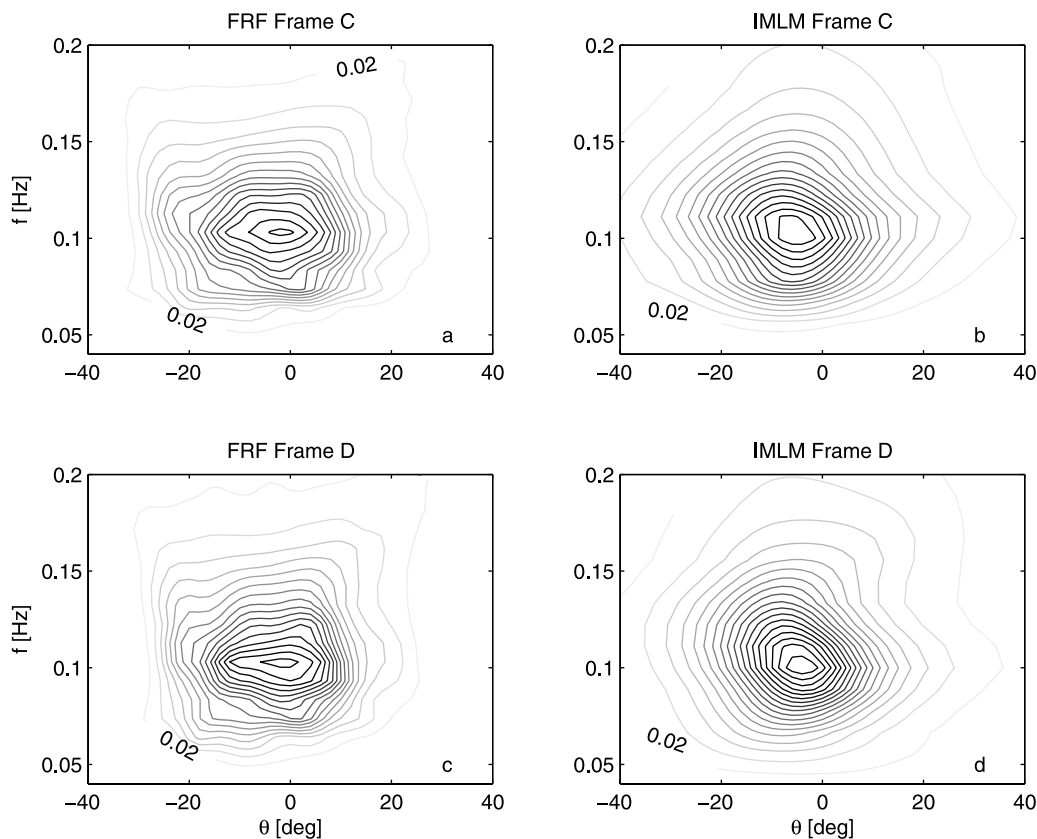


Figure 13. Average normalized wave directional spectra for all cross-ripple occurrences at frames (a and b) C and (c and d) D. The 8-m array directional spectra have been shoaled from the 8 m isobath to the frame positions and transformed to the seabed using linear wave theory.

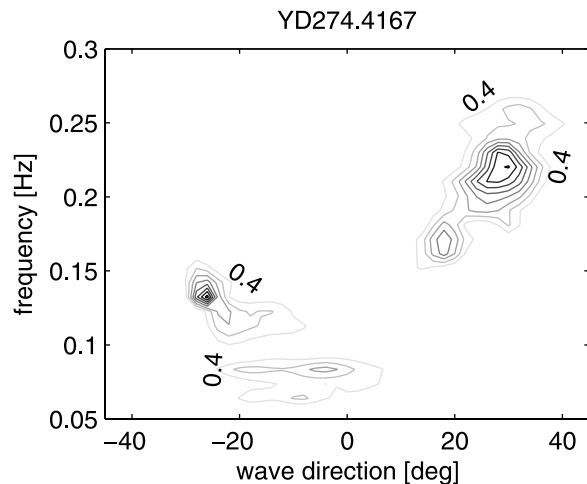


Figure 14. Bimodal wave directional spectrum corresponding to a cross-ripple occurrence at frame D. Directional spectrum is from the U. S. Army Corps of Engineers Field Research Facility (FRF) 8-m array shoaled to frame D's location.

case a spectrum which is bimodal both in f and θ . Figure 15 is an example of a unimodal directional spectrum during a cross-ripple occurrence.

[23] There were 82 and 89 directional spectra from the 8-m array during cross-ripple occurrences at frame C and D, respectively. Table 2 lists the percentages of these spectra determined to be bimodal in direction or frequency or to be unimodal. At both frames C and D, only 17% were bimodal in direction. In contrast, 65% and 67% were bimodal in frequency at frames C and D, respectively, while 32% and 35% were unimodal. (Note that some of the directional spectra were bimodal in both frequency and direction, so the sum of the percentages can exceed 100%). In addition, the 1-D integrals of the directional spectra (equations (3) and (4)) were also examined visually to determine if a given spectrum was bimodal in either frequency or direction.

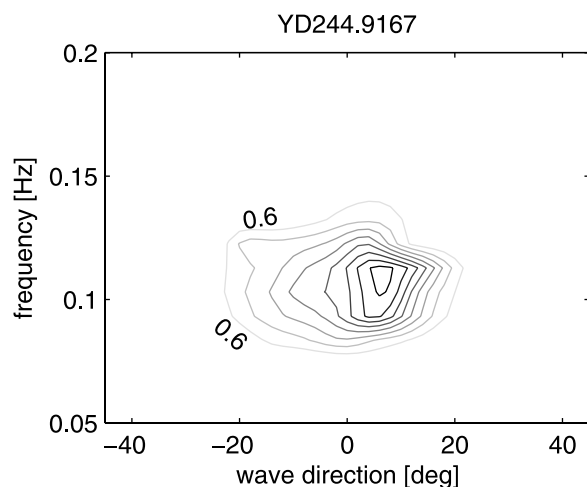


Figure 15. Unimodal wave directional spectrum corresponding to a cross-ripple occurrence at frame C. Directional spectrum is from the FRF 8-m array shoaled to frame C's location.

Table 2. FRF Directional Spectra Statistics During Cross-Ripple Occurrences^a

	FRF 8 m		p_{uv}	
	Frame C $N = 82$	Frame D $N = 89$	Frame C $N = 474$	Frame D $N = 390$
			<i>Bimodal</i>	
θ (auto)	17%	17%	2%	3%
θ (visual)	23%	20%	–	–
f (auto)	67%	65%	47%	40%
f (visual)	58%	52%	–	–
			<i>Unimodal</i>	
(auto)	32%	35%	53%	60%
(visual)	30%	36%	–	–

^aFRF is U. S. Army Corps of Engineers Field Research Facility. N is the total number of directional spectra during cross-ripple occurrences.

These results are also listed in Table 2. The visually determined numbers are similar to those determined automatically.

[24] The results from the automatic bimodality determination for the p_{uv} spectra are also listed in Table 2. (Because of the large number of spectra, visual measures of bimodality were not made for the p_{uv} data.) At frames C and D, 47% and 40% of the p_{uv} spectra were found to be bimodal in frequency, respectively, comparable to, but less than, the 65% to 67% values obtained from the 8-m array data. Only 2–3% of the p_{uv} spectra were bimodal in direction, substantially less than the 17% value for the shoaled 8-m array spectra. The difference reflects the relatively coarse angular resolving power of the single-point p_{uv} sensors compared to that of the 8-m array.

[25] Figure 16 shows the angle differences, $|\theta_a - \theta_b|$, between the peaks in the 26 directionally bimodal shoaled spectra from the 8-m array. The subscripts a and b denote the more and less energetic of the two peaks, respectively. The $|\theta_a - \theta_b|$ distribution is broad, reaching values as high

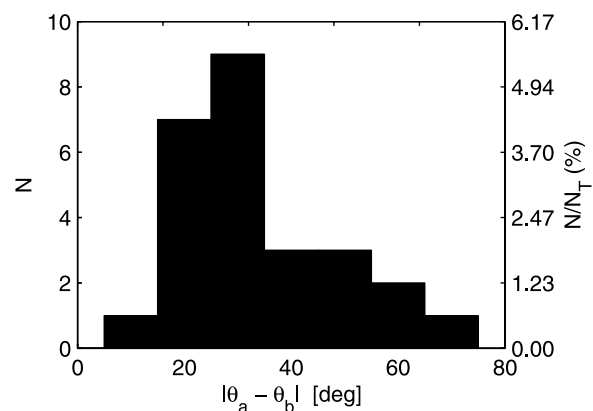


Figure 16. Histogram of the differences between the direction, θ_a , of the more energetic peak and, θ_b , that of the less energetic peak, in the 26 shoaled directional spectra from the 8-m array which were bidirectional. θ_a and θ_b were determined from the 1-D integral over frequency (equation (3)). Note that these 26 instances represent only 17% of the $N_T = 171$ spectra from the 8-m array corresponding to cross-ripple occurrences (Table 2), as reflected by the percentages on the right-hand axis.

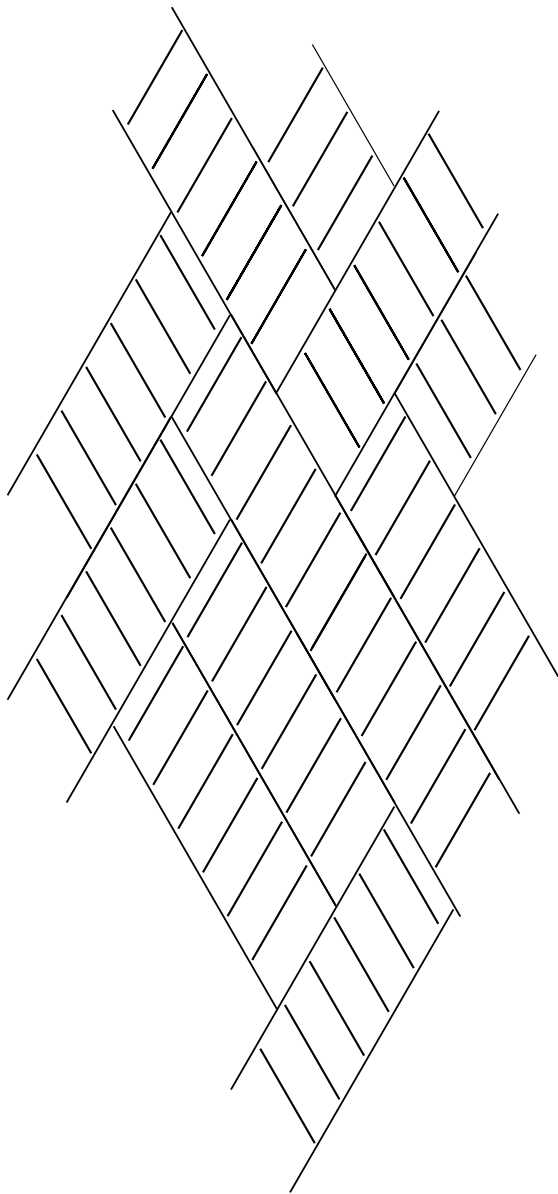


Figure 17. Cartoon depicting a cross-rippled bed with two long-crested components oriented at $\pm 30^\circ$ with respect to the incident wave direction (arrow). The angle formed by the long- and short-crested components is approximately 60° . The pattern was constructed from variable-length tiles like that in Figure 9. Note the quasi-regular diamond-shaped pattern formed by the long-crested ripples, consistent with the sonar images.

as 70° . While there is a peak in the distribution near 30° which one might be tempted to associate with the peaks in ψ_L (Figure 10), note that (1) the data in Figure 16 represent only 17% of the spectra from the 8-m array; (2) the remaining 83% were unimodal in direction; and (3) the sum of all occurrences in Figure 16 at separation angles outside the $30^\circ \pm 5^\circ$ interval is 17, i.e., nearly twice the number within the interval.

[26] Thus, briefly summarizing, these results indicate that bidirectional incident waves are not a necessary feature of

the hydrodynamic conditions under which cross ripples occur.

4. Discussion

[27] The sonar images and their 2-D spectra indicate that the longer wavelength component occurred with two crest orientations, located at approximately $\pm 30^\circ$ from shore normal, resulting in a diamond-like pattern at meter-scales. The $\sim 60^\circ$ angle between two obliquely oriented long-wavelength components was approximately bisected by the peak in the distribution of incident wave directions (Figure 10). At Queensland Beach, Nova Scotia, *Smyth et al.* [2002] (Figure 1b) present a sonar image of cross ripples that shows two long-crested ripples oriented obliquely to the incident waves.

[28] The angle formed by the short- and long-crested ripple components was visually estimated to be about 60° also (Figure 8b). These results lead to the conceptual view of a cross-rippled bed presented in Figure 17. This pattern was constructed by tiling, each “tile” being like the ladder segment in Figure 9, but of variable length. The rails cross or intersect at a 60° angle, thus forming an irregular diamond-like lattice.

[29] The pattern sketched in Figure 17 is different from the “long, straight, uninterrupted crests” reported by *Clifton et al.* [1971] for the long-wavelength component. However, in their cartoon illustrating the shoreward bed form sequence, *Machida et al.* [1974] depicted intersections between the long-crested components of their cross ripple-like feature. Also, a sonar image of a cross-rippled bed at Queensland Beach, NS [*Crawford and Hay*, 2001, Figure 6a] contains a diamond-like feature formed by the long-crested components.

5. Conclusions

[30] Results have been presented from an investigation of cross-ripple occurrence and pattern in rotary sonar imagery collected in approximately 3-m water depth over a 10-week period during the SandyDuck97 nearshore dynamics experiment. As reported previously by *Hay and Mudge* [2005], cross ripples occurred during all of the 11 main storm events, typically during both the wave growth and decay phases of each event, and at intermediate wave energies (significant near-bed wave orbital velocities ~ 40 cm/s on average). The mean cross-shore and longshore currents were comparatively weak, ranging between ± 5 cm/s and ± 10 cm/s, respectively.

[31] The cross-ripple pattern revealed in the sonar imagery is made up of long-crested “rails” and shorter-crested, shorter-wavelength “rungs” arranged in a ladder-like pattern, consistent with previous descriptions based on visual observations [*Clifton et al.*, 1971; *Machida et al.*, 1974; *Clifton*, 1976]. Also consistent with previous reports are the observed wavelengths of the two ripple sets: 30 to 55 cm on average for the long-crested set and close to 10 cm for the short-crested set. On horizontal scales extending up to 10 m (the diameter of the sonar images), however, the present observations indicate that the long-crested ripple components occur at two dominant orientations, intersecting at an angle of approximately 60° . The result is an irregular

diamond-like pattern at $O(1)$ m scales. In addition, the short-crested rungs tended to be oriented at an acute angle (also approximately 60°) to the longer-crested rails. Thus, the conceptual picture of the cross-ripple pattern that emerges from these data is a quasi-regular lattice structure built up of ladder-like tiles of variable length and oriented at approximately $\pm 30^\circ$ from the axis of symmetry (corresponding on average to the shore normal). This pattern is different from that sketched in the work of Clifton [1976], in which the ladder-like features remain parallel but is comparable to the drawing in the work of Machida *et al.* [1974] which shows similarly truncated ladders at what appear to be two dominant orientations.

[32] Wave directional spectra in the sea-and-swell band were determined for the sonar locations from local puv measurements and, after accounting for the effects of shoaling assuming constant cross-shore energy flux and linear wave theory, from the 8-m array directional spectra. Within the expected approximately $\pm 5^\circ$ accuracy of the instrument and frame orientations, both the dominant wave direction (determined from the correlation between locally measured u and v), and the peak wave direction (determined from the shoaled 8-m array directional spectrum), approximately bisected the angle between the two long-crested ripple components. While this result is consistent with the qualitative observations of wave direction relative to cross-ripple crests made by Clifton *et al.* [1971], to our knowledge the present study represents the first quantitative determination of cross-ripple orientation relative to the directional distribution of the incident waves.

[33] The average of the wave directional spectra over all cross-ripple occurrences was unimodal in both energy and direction, and the directional spread was typically less than or equal to 30° (full width at half maximum). Even in the relatively few cases when the wave spectra were directionally bimodal (17% based on the 8-m array), the directional separation between the two energy peaks was broadly distributed between 10° and 70° . Thus, the present results demonstrate that wave trains propagating from two different directions are not only not required for cross-ripple formation but also were not observed for the majority of the cross-ripple occurrences.

[34] The angle between the long-crested components was also examined in relation to the mean longshore and cross-shore currents. No tendency was found for the orientations of the long-wavelength crests to change with \bar{u} or \bar{v} .

[35] In conclusion, the present investigation of cross-ripple occurrence and pattern in relation to wave directional spectra has revealed nothing obviously special about the directional properties of the incident waves. Neither do mean currents have any discernable effect on cross-ripple orientation. Thus, the present results indicate again, as in the work of Hay and Mudge [2005] but now including principal wave direction among the forcing parameters, that wave energy is the dominant controlling factor for cross-ripple occurrence. There remains the possibility that the directional

spread of the incident waves is important, as suggested by Allen's remark on short-crestedness, cited in section 1. This possibility is beyond the scope of the present paper and is deferred until later.

[36] **Acknowledgments.** The authors would like to thank the Bill Birkemeier and the FRF staff for making available the bathymetry and 8-m wave directional spectra and Tom Herbers for useful discussions on directional spreading and directional spectral estimation. This research was funded by the Coastal Geosciences Program of the U. S. Office of Naval Research and the Natural Sciences and Engineering Research Council of Canada.

References

- Allen, J. R. L. (1984), *Sedimentary Structures: Their Character and Physical Basis*, Elsevier, New York.
- Birkemeier, W. A., H. C. Miller, S. D. Wilhelm, A. E. DeWall, and C. S. Gorbics (1985), A user's guide to the Coastal Engineering Center's (CERC's) Field Research Facility, *Tech. Rep. CERC-85-1*, 137 pp., Coastal Eng. Res. Cent., U.S. Army Corps of Eng., Vicksburg, Miss.
- Bowen, A. J. (1969), The generation of longshore currents on a plane beach, *J. Mar. Res.*, *27*, 206–215.
- Clifton, H. E. (1976), Wave-formed sedimentary structures - A conceptual model, in *Beach and Nearshore Sedimentation*, edited by R. A. Davis Jr. and R. L. Ethington, *SEPM Spec. Publ.*, *24*, 126–148.
- Clifton, H. E., and J. R. Dingle (1984), Wave-formed structures and paleoenvironmental reconstruction, *Mar. Geol.*, *60*, 165–198.
- Clifton, H. E., R. E. Hunter, and R. L. Phillips (1971), Depositional structures and processes in the non-barred high-energy nearshore, *J. Sediment. Petrol.*, *41*, 651–670.
- Crawford, A. M., and A. E. Hay (2001), Linear transition ripple migration and wave orbital velocity skewness: Observations, *J. Geophys. Res.*, *106*, 14,113–14,128.
- Doucette, J. S. (2000), The distribution of nearshore bedforms and effects on sand suspension on low-energy, micro-tidal beaches in Southwestern Australia, *Mar. Geol.*, *165*, 41–61.
- Fofonoff, N. (1969), Spectral characteristics of internal waves in the ocean, *Deep Sea Res.*, suppl., *16*, 58–71.
- Hay, A. E., and T. Mudge (2005), Principal bed states during Sandy-Duck97: Occurrence, spectral anisotropy, and the bed state storm cycle, *J. Geophys. Res.*, *110*, C03013, doi:10.1029/2004JC002451.
- Hay, A. E., and D. L. Wilson (1994), Rotary sidescan images of nearshore bedform evolution during a storm, *Mar. Geol.*, *119*, 57–65.
- Henderson, S. M., and A. J. Bowen (2002), Observations of surf beat forcing and dissipation, *J. Geophys. Res.*, *107*(C11), 3193, doi:10.1029/2000JC000498.
- Herbers, T. H. C., S. Elgar, and R. T. Guza (1999), Directional spreading of waves in the nearshore, *J. Geophys. Res.*, *104*, 7683–7693.
- Jenkins, F. A., and H. E. White (1957), *Fundamentals of Optics*, 637 pp., McGraw-Hill, New York.
- Long, C. E. (1991), Index and bulk parameters for frequency-direction spectra measured at CERC Field Research Facility September 1986 to August 1987, *Tech. Rep. MR 91-6*, Coastal Eng. Res. Cent., U.S. Army Corps of Eng., Vicksburg, Miss.
- Machida, T., M. Inokuchi, E. Matsumoto, T. Ishii, and H. Ikeda (1974), Sand ripple patterns and their arrangement on the sea bottom of the Tatado Beach, Izu Peninsula, Central Japan, *Sci. Rep. Tokyo Kyoiku Daigaku Sect. C*, *112*, 1–16.
- Oltman-Shay, J., and R. T. Guza (1984), A data-adaptive ocean wave directional-spectrum estimator for pitch and roll type measurements, *J. Phys. Oceanogr.*, *14*, 1800–1810.
- Smyth, C., A. E. Hay, and L. Zedel (2002), Coherent doppler profiler measurements of near-bed suspended sediment fluxes and the influence of bedforms, *J. Geophys. Res.*, *107*(C8), 3105, doi:10.1029/2000JC000760.

R. A. Cheel and A. E. Hay, Department of Oceanography, Dalhousie University, Halifax, NS B3H 4J1, Canada. (richard.cheel@dal.ca; alex.hay@dal.ca)